NANO MICRO small

Supporting Information

for *Small,* DOI: 10.1002/smll.201703683

Smart-Dust-Nanorice for Enhancement of Endogenous Raman Signal, Contrast in Photoacoustic Imaging, and T2-Shortening in Magnetic Resonance Imaging

*Christoph Pohling, Jos L. Campbell, Timothy A. Larson, Dominique Van de Sompel, Jelena Levi, Michael H. Bachmann, Sarah E. Bohndiek, Jesse V. Jokerst, and Sanjiv S. Gambhir**

Supporting Information

Smart-Dust-Nanorice for Enhancement of Endogenous Raman Signal, Contrast in Photoacoustic Imaging and T2-shortening in Magnetic Resonance Imaging

C. Pohling 1, J.L. Campbell 1, T.A. Larson 1, D. Van de Sompel 1, J. Levi 1, M.H.Bachmann 2, Sarah E. Bohndiek 1, J.V. Jokerst 2, and S.S. Gambhir* 1

Stanford School of Medicine, 1 Department of Radiology, 2 Department of Pediatrics,
Clark Center E150, 318 Campus Drive, Stanford, CA 94303, USA

S0: Abstract

The following sections provide additional information to the main article. We address historical aspects of colloidal gold solutions and provide control experiments that are an essential part for evaluating the results of our SERS particles.

S1: Brief review about SERS particles and examples of nearfield simulations

The strong optical absorption associated to SPRE's gives rise to the brilliant color of colloidal gold solutions. According to that, plasmonic nanoparticles show a remarkable history and were already explored at the end of the 19th century, long before SERS effects became relevant for Raman spectroscopy.[1] The accurate understanding of a material's extinction, absorption, scattering and SPRE has been addressed for multiple topics in physics and engineering.[2] Gustav Mie provided the analytical theory for spherical particles in 1908 [3] and nowadays, methods such as the Finite Element Method (FEM) enable to solve for complex sample structures of arbitrary shape.[4] In the main article, Comsol MultiphysicsTM software has been used to simulate the nearfield patterns of SDN where the electric properties of several materials were taken into account. Open source code also exists, such as "DDSCAT" that has been written by Bruce T. Draine and P. Flateau.[5] The code is based on the so-called Discrete Dipole Approximation (DDA) where "targets" (nanoparticles) are

approximated by arrays of polarizable points. Please see Karamehmedović *et al.*[6] for a detailed comparison between different software environments for SPRE simulation. For this supporting information, we performed simulations by using DDSCAT, a highly sophisticated open-source platform for calculation of scattering phenomena. We illustrate properties of simple spheres such as the "smart-dust" basis particle. Matlab® software (MathWorks) was used for visualization of the output files although the authors also refer to freeware such as Paraview© (Sandia Corporation, Kitware Inc.) that also worked well (data not shown). The results of simulating a single gold sphere (represented by 6575 individual dipoles according to the DDA approach) are shown in **Figure S1**. The electromagnetic wave travels along the x-axis and the electric field $\vec{E}$ is polarized in the xy-plane, see also the arrows marked by the symbols for the wavevector $\vec{k}$ and $\vec{E}$. **Figure S1 a)** shows a typical dipole pattern resulting from excitation at 532 nm which is close to the optical absorption-maximum. **Figure S1 b)** simulates excitation at 785 nm, as conducted in our experiment. As it can be seen, the near-field enhancement is lower. **Figure S1 c)** and **d)** finally show how SERS effects change while increasing the size of the sphere: As explained by spherical-harmonics[7] the formation of multipole field patterns occurs in case of larger particles. The sphere shown in **Figure S1 c)** (diameter of 120 nm) represents the "transition" between a dipole- and a quadrupole- pattern while **Figure S1 d)** finally shows a nearfield effects purely dominated by the quadrupole resonance. The amount of enhancement is moderate in these four examples. However, the situation dramatically changes when a second particle is included. **Figure S1 e)** shows a dimer of 50 nm-spheres that are separated by 10 nm. The field strength within the "gap" is already an order of magnitude higher than in any of the examples above. Those high-intensity gaps in a SERS substrate are called "hot spots". DDSCAT not only calculates for the nearfield effects at a given wavelength, the absolute scattering cross section of the "target" is calculated as well. Hence, a frequency sweep has been performed for multiple wavelengths of the visible

spectral region in order to obtain a theoretical spectrum of the optical absorption, see **Figure S1 f)**. The calculated values (blue dots, the absolute absorption cross section is divided by particle cross section and plotted against the excitation wavelength) is overlaid with the measured (and scaled) absorption spectrum of an aqueous solution of 50 nm gold spheres that we obtained by using the citrate reduction method[8] (black line, scaled OD against wavelength). The curves show a very good agreement besides a slightly different maximum, suggesting that the spheres of the experimental batch are a larger than 50 nm. The broader absorption band also indicates a certain distribution of sizes. The same simulation procedure has been repeated for a target representing a dimer of spheres (red dotted line, only one orientation relative to the exciting field has been considered). The curve reveals an absorption shift by about 50 nm. While the nearfiled patterns help understanding the different enhancement effects of isolated and agglomerated spheres, the simulated absorption spectra are an excellent tool for evaluating the overall quality of a chemical synthesis of spherical plasmonic nanoparticles. While resonance conditions of nanospheres can be experimentally monitored via optical absorbance spectroscopy, SERS processes are complex in case of hot-spot dominated systems and the excitation wavelength for optimal Raman signal output does not necessarily correlate with the optical absorbance maximum of the SERS agent. Please see Kleinmann *et al.* for detailed discussions about the relations between excitation wavelength, optical absorption and SERS effects.[9]

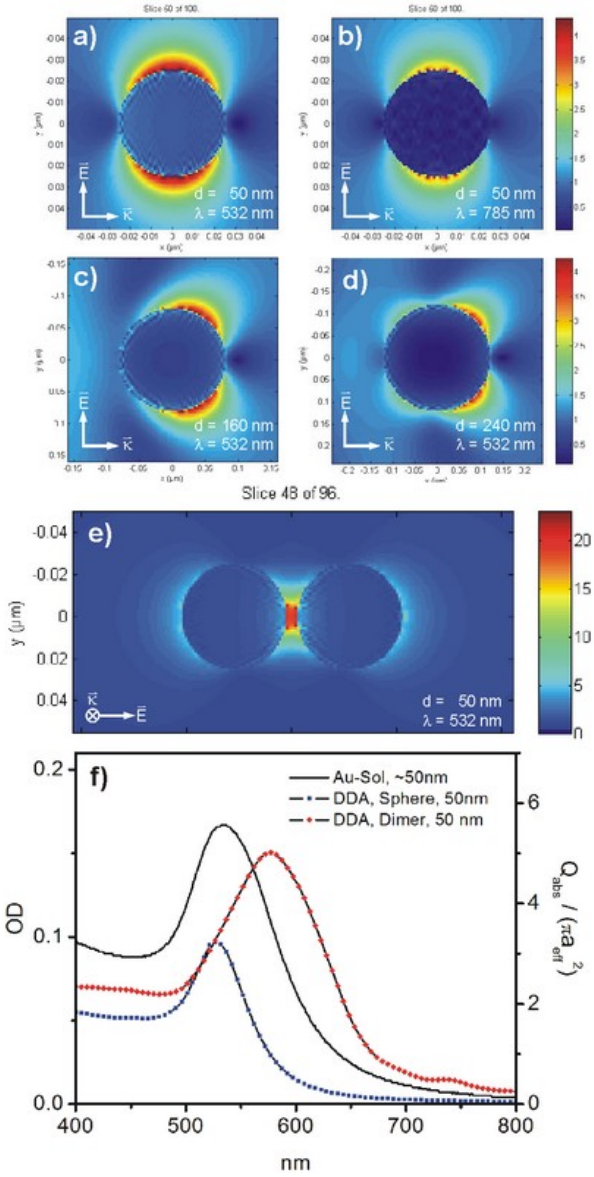

Figure S1: a) DDSCAT nearfield calculation of a 50 nm gold sphere in vacuum with excitation at 532 nm (6575 dipoles). b) Scattering problem as in a), with 785 nm excitation. c) 160nm-sphere at 532 nm excitation. d) 240nm-sphere at 532nm excitation. The transition from dipole to quadrupole resonance is clearly visible. e) The scattering problem of a) has been expanded to a dimer of spheres, with a distance of 10 nm. The local field intensity between the spheres is an order of magnitude higher. f) The experimentally collected UV-Vis spectrum of a colloidal solution of silica-coated 50 nm spheres (black line) as well as the DDSCAT calculation of the absolute scattering cross section of a 50 nm gold sphere in water for multiple excitation wavelengths (blue dots) and a dimer of spheres (red dots).

S2: Deposition of ultrafine gold sol on hematite spindles

During the SDN synthesis, the products of each step have been carefully monitored. TEM was the first choice for visualizing hematite spindles and the growth of a closed gold shell. As an example, **Figure S2 a)** shows a high resolution TEM image of plain hematite particles before seed coating by ultrafine gold. The Duff-particles, however, are very small and therefore provide only low contrast in TEM, see also **Figure 2 b)**. Nevertheless, it is possible to estimate a successful gold-predeposition on the ironoxide-surface by TEM, as shown in **Figure S2 c)**, where the gold spheres appear as small granular structure on the surface of the ironoxide. This structure is not present in a). Validating the correct size of the ultrafine gold-sol and a successful predeposition on the hematite surface is crucial for the success of the final step of gold coating by electroless deposition. If the seed particles were too big, the next step resulted in formation of larger gold-spheres rather than growth of a closed shell. However, and as described in the original literature, UV-VIS spectroscopy is ideally used for monitoring the size of the fresh, ultrafine Duff-particles; as long as the particles are small (~5 nm), no plasmonic effects take place. With increasing particle size, the typical absorption band around 510 nm becomes visible. This can either be an effect of adding too much hydrochlorauric acid during synthesis or just by aging of the solution. It is crucial to validate the correct particle size (the absence of any plasmon absorption in the UV-VIS spectrum) before using the gold sol for surface functionalization of the ironoxide cores. **Figure S2 d)** shows different absorption spectra of Duff-particles where the amount of hydrochlorauric acid has been reduced for each batch. Only the lower curve relates to a particle size small enough for successful Nanorice fabrication. We performed such a “gold-quantity sweep” as a simple and fast control for each new batch of Duff-particles (and hydrochlorauric acid stock solution) that was fabricated. The given quantities (mL) refer to a specific run in our lab and are not representative, please see Duff et al. for data about the absolute concentration. We observed

the validated batches of ultrafine gold sol to be storable for at least one week at 5°C and protected from light. Freshly prepared batches also worked well.

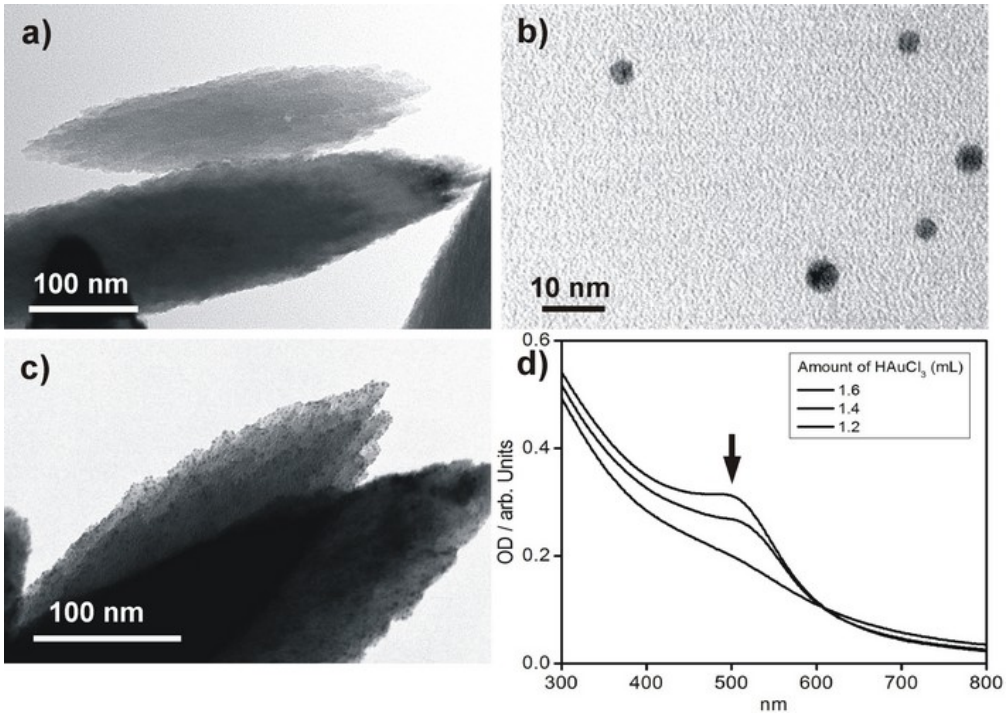

Figure S2: a) TEM image of the spindle-shaped hematite particles before surface functionalization. b) ultrafine gold-spheres (~ 5nm in Diameter) obtained by the Duff-method. c) The hematite particles after surface functionalization by APTMS and the ultrafine gold sol shown in b). The ultrafine spheres appear as a dotted structure on the surface that is not present in a) where the plain ironoxide is shown. d) UV-VIS spectrum of three different batches of ultrafine gold particles obtained from the Duff method. The amount of $HAuCl_3$ (mL) has been reduced each time. In case of excessive gold, the particle size is larger than ~5 nm which results in plasmon absorption. The absence of such a band around 510 nm is the benchmark for a successful synthesis of the desired size.

S3: Control experiment, a simple AB-case of SDN application

For validating the ability of SDN to act as "spray-on, general-purpose" agent for Raman signal enhancement, we defined a control experiment with two different types of sample molecules. This "AB-case" is a model environment, where the type of sample molecules is precisely controlled and reference spectra of each sample were collected in advance. A standard quartz slide was coated by films of Glucose and Polyvinyl-alcohol (PVA). In a first step, Raman scanning was performed on an area of 5mm times 5mm that contained sections of both films. Spectra were collected at a laser power of 1% of its maximal value and at a pixel dwell time of one second. Reference spectra were collected at an acquisition time of 5 seconds per spectrum. An overlay of brightfield- and Raman image is shown in **Figure S3 a)**. The Raman image is shown as red inset with thermal color scheme of maximum intensity projection after full spectral binning. The brightfield image is shown as greyscale. The films of glucose and PVA appear in the upper and lower half of the scanned area. The scan was repeated after airbrush-coating with SDN. The spectral results are shown in **Figure S3 b)** and **c)** for glucose and PVA, respectively. The reference spectra are plotted in the upper lines (green: Glucose, blue: PVA). Average spectra (of 3316 spectra) are plotted in red for SDN-enhanced signals (middle line) and in dark grey for a control scan, performed before SDN was applied (lower line). In both cases, the signals from the untreated sample show a poor signal to noise ratio and are missing several vibrational features. After SDN coating, strong signals appear and in case of glucose, the result perfectly agrees with the intrinsic reference. In case of PVA, the SERS spectrum shows some deviations/additional features at 800-, 1200- and 1350 cm^{-1} that might occur due to symmetry effects or impurities of the film on a nanometer-scale. To sum up, in both cases SDN coating of an existing sample provides strong Raman signals that can be correlated to the sample molecules.

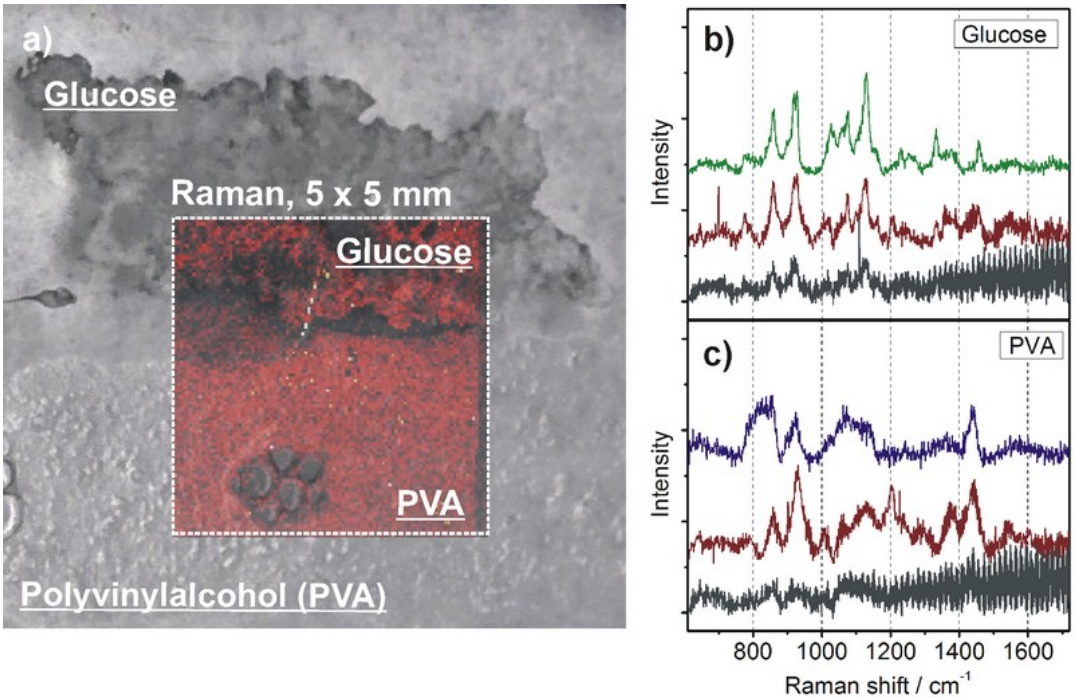

Figure S3: a) Brightfield image of a film of Glucose in the upper half and Polyvinyl-alcohol (PVA) in the lower half of the image, superimposed by the maximum intensity projection of a Raman scan performed over the border between both films (red inset). b) Reference spectrum of plain glucose (upper line, green) and average spectrum of the glucose-containing sample in the presence (middle line, red) and absence (lower line, grey) of SDN. c) Results for PVA, plotted in the same scheme as in b).

S4: Background signals of SDN

During the synthesis of SDN, APTMS is used in excess for surface functionalization of the ironoxide-core. One could assume that these molecules (and other residual molecules) can act as (unwanted) Raman marker molecules once they get incorporated into the SERS substrate. The following experiment was made to reveal potential side effects: An aqueous suspension of plain SDN has been sprayed on a quartz slide. An area of 100 µm times 100 µm was Raman scanned at a step size of 1 µm. Brightfield image and Raman result (maximum intensity projection at 1450 cm^{-1}) are shown in **Figure S4 a)**. The brightfield image shows agglomerates of SDN particles (bright yellowish structures). The Raman result (dashed square and red inset) shows weak unspecific structures. Besides an average spectrum, four individual single-shot SERS spectra have been selected for further discussion. The spectral results are

shown in **Figure S4 b)**, starting with the average spectrum shown in red (upper line, average of 10201spectra), a reference spectrum of APTMS (plotted in blue, second line from top) followed by the four single spectra collected at the white squares labelled by 1-4 in **Figure S4 a)**. As it can be seen, the average spectrum is free of any strong spectral features. This is different from any of our results above, where sample molecules were present. Therefore, this experiment can be considered as a proper negative control. However, weak signals (about 200 counts CCD) are present at some spectral positions. As expected, they can be explained by the reference spectrum of APTMS which is still present within SDN particles. The four additional single-shot SERS spectra that were selected from the data are shown in the lower lines of **Figure S4 b)**. In these cases, and besides that the signal intensity is very low, they do not show a common signature which explains why the global average is almost free of unwanted signals. To conclude, the background signal of SDN is low, which fulfills a basic requirement for a SERS agent that aims for enhancement of intrinsic spectra of the sample.

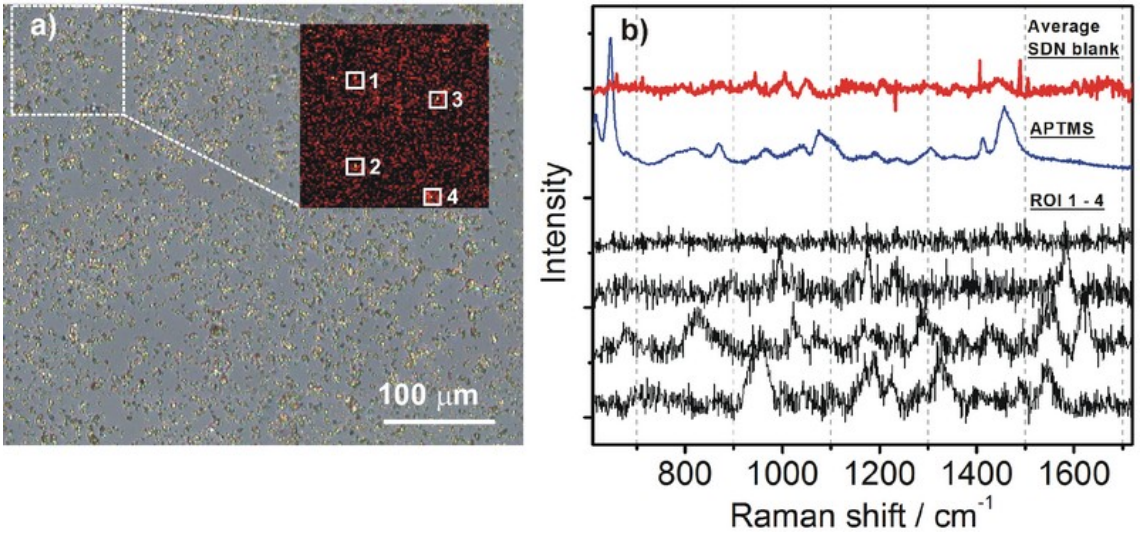

Figure S4: a) brightfield image of plain SDN on glass with a Raman-scanned area in the upper left (dashed white frame) and the resulting maximum intensity projection at 1450 cm^{-1} shown in the upper right. At four positions marked by white squares (1-4), individual spectra were collected for further discussion. b) The spectral results of a) are plotted, together with a reference spectrum of APTMS. Starting from the top to bottom: Average spectrum of the Raman data (red line), reference spectrum of APTMS (blue line) and four individual spectra (black lines).

S5: SERS using smart dust particles (silica coated spheres)

This section shows results of smart dust particles on COS cells. Smart dust was successfully synthesized according to the protocol that Li *et al.* recently presented.[10] An absorption spectrum of the gold spheres is shown in **Figure S1 f)** while the final product was validated by TEM, please see **Figure S5 a)**. A droplet of aqueous particle suspension (5 µL) was allowed to dry on a layer of COS-cells, followed by a Raman scan of 101x101 spectra at a step size of 100 µm. The acquisition time was set to 10 seconds per spectrum at a laser power of ~ 2 mW. **Figure S5 b)** shows the result of a maximum intensity projection at 1450 cm^{-1}. The area where the droplet has dried is clearly visible due to the large amount of bright pixels (yellow to white) that indicate successful SERS events. The spectral intensities at these points are much higher than from areas of the untreated COS-layer (dark red). Due to drying effects, particles seem more concentrated at the borders. Finally, averages (80 spectra) collected in a region of interest (ROI) outside of the particle-treated area (ROI 1, grey box) were compared with spectra collected inside (ROI 2, grey box), please see **Figure S5 c)**. The reference spectrum is shown in black while the result of smart-dust-covered cells is shown in red. The spectral intensity of the latter one is reasonably higher and nicely matches the spontaneous Raman reference between 900 cm^{-1} and 1500 cm^{-1}. To sum up, we observed that smart dust is a highly SERS-active compound and validated its ability to reasonably enhance intrinsic Raman signatures of our sample (cell-layer). Unfortunately we could not compare these results directly to SDN, e.g. due to differences in particle concentration, application and substrate-quality. Any comparison was based on the nearfield properties that were accessible by the FEM-simulations shown above.

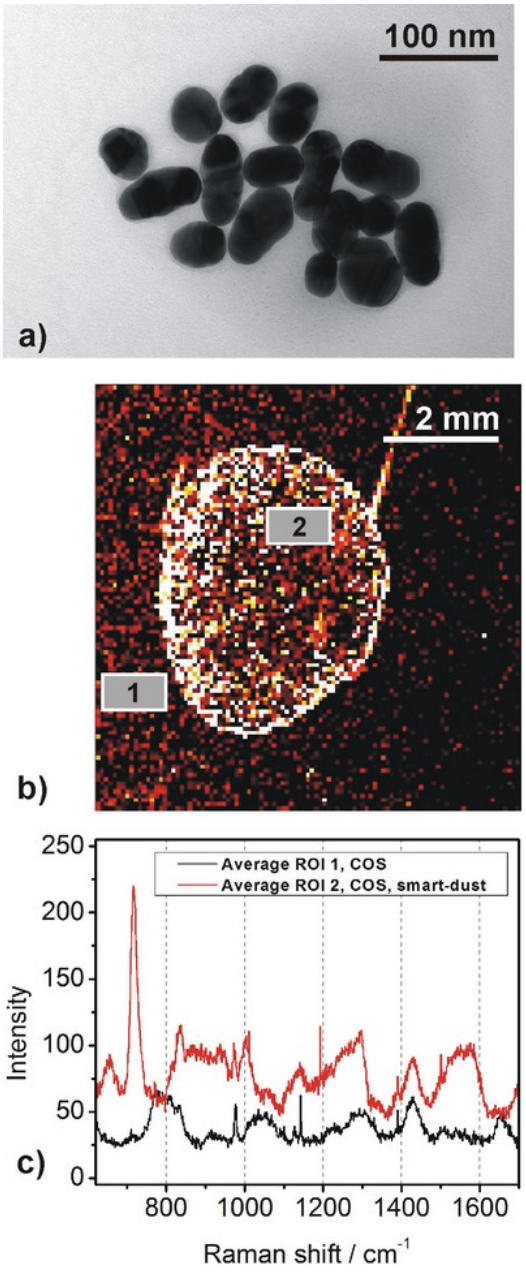

Figure S5: a) TEM-image of smart dust spheres, synthesized according to the description of Li *et al*. The silica coating appears as a grey layer encapsulating the particles. b) Raman result as maximum intensity projection at 1450 cm^{-1}. Multiple SERS events appear as bright pixels in an area, where a droplet of smart dust solution was applied in advance. c) Average spectra from ROI 1 and ROI 2 in b) with untreated cells (black line) and cells covered by smart dust (red line). The spectral intensity is higher while multiple Raman features of the reference spectrum are present in the SERS-result.

References Supporting Information

[1] a) W. Naumoff, *Zeitschrift für anorganische Chemie* **1914**, *88*, 38; b) R. Zsigmondy, *Justus Liebigs Annalen der Chemie* **1898**, *301*, 29.

[2] M. L. Walker, *Dept. of Materials Science and Engineering* **2012**, *MS*.

[3] G. Mie, *Annalen der physik* **1908**, *330*, 377.

[4] P. Monk, *Finite element methods for Maxwell's equations*. Oxford University Press: **2003**.

[5] a) B. T. Draine, *The Astrophysical Journal* **1988**, *333*, 848; b) B. T. Draine,P. J. Flatau, *JOSA A* **2008**, *25*, 2693; c) P. Flatau,B. Draine, *Opt. Express* **2012**, *20*, 1247; d) P. J. Flatau,B. Draine, *J. Opt. Soc. Am. A* **1994**, *11*, 1491; e) J. Goodman, B. T. Draine,P. J. Flatau, *Opt. Lett* **1991**, *16*, 1198.

[6] M. Karamehmedović, R. Schuh, V. Schmidt, T. Wriedt, C. Matyssek, W. Hergert, A. Stalmashonak, G. Seifert,O. Stranik, *Optics express* **2011**, *19*, 8939.

[7] K. L. Kelly, E. Coronado, L. L. Zhao,G. C. Schatz, *The Journal of Physical Chemistry B* **2003**, *107*, 668.

[8] G. Frens, *Nature* **1973**, *241*, 20.

[9] a) S. L. Kleinman, R. R. Frontiera, A.-I. Henry, J. A. Dieringer,R. P. Van Duyne, *Physical Chemistry Chemical Physics* **2013**, *15*, 21; b) S. L. Kleinman, B. Sharma, M. G. Blaber, A.-I. Henry, N. Valley, R. G. Freeman, M. J. Natan, G. C. Schatz,R. P. Van Duyne, *Journal of the American Chemical Society* **2012**, *135*, 301.

[10] J. F. Li, Y. F. Huang, Y. Ding, Z. L. Yang, S. B. Li, X. S. Zhou, F. R. Fan, W. Zhang, Z. Y. Zhou,B. Ren, *nature* **2010**, *464*, 392.